Chapter III

Applications of the Lateral Derivative Method

The development of the lateral derivative method contains three major assumptions as discussed in section 2.1. These are: 1) the lateral slowness function to a given event can be approximated over the distance of a cable-length by a second-order Taylor-series expansion about every midpoint; 2) the slowness is invariant with depth; and 3) the raypaths are straight. The purpose of the first three sections of this chapter is to test these assumptions by applying the lateral derivative method to three different synthetic models. Moreover, the implementation of the lateral derivative method requires the choice of a stabilization parameter, ϵ, [see equation (2.31)], and we will also investigate the influence of different values of ϵ on the inversion. The fourth section will discuss the implementation of the lateral derivative method on field data. The field data are taken from a marine survey off the coast of Newfoundland and have a substantial lateral velocity variation due to the seafloor topography.

3.1. Synthetic Model 1

The purpose of the first synthetic model is to test the LDM over an area where the Taylor-series approximation for the lateral slowness is not valid at every midpoint. The most severe case of this is where the velocity changes abruptly between two midpoints as would be the case over a vertical fault. Figure 3.1 shows such a model (referred to as Model 1) which consists of two homogeneous mediums of velocities v_1 and v_2 feet/sec overlying a horizontal reflector at depth z feet and separated by a vertical boundary at x = 10100 feet. Although the velocity changes too rapidly to be accurately described in the vicinity of every midpoint by a second-order Taylor-series expansion, it does satisfy the assumption of vertical velocity homogeneity. From the results of section 2.2, we cannot expect to recover the high spatial frequencies of the lateral slowness function. The question to be

answered, however, is: does the LDM do any better than conventional velocity estimation?

The LDM will be tested on three different combinations of v_1, v_2, and z. These are given in the following table.

case	v_1	v_2	z
1	8000	9000	5000
2	8000	9000	10000
3	8000	10000	5000

For each of these cases, the LDM will be tested for three different values of the stability parameter, ϵ. Before discussing each case individually, some general comments pertaining to the solution with the LDM are as follows. The input data were extended to 512 midpoints to avoid any problem with boundary conditions. Secondly, before computing the second derivative of the conventional slowness estimates, these estimates were first averaged over a cable-length. Lastly, the finite-difference spacing used was one-fourth of a cable-length.

Using a ray-tracing program the traveltimes for each case were computed for common-midpoint gathers for the midpoints shown in Figure 3.1. The common-midpoint gathers are 24-fold with a near and far full offset of 400 and 9600 feet respectively. A midpoint spacing of 200 feet makes the cable-length equal to 48 midpoints in Figure 3.1. For each case a conventional velocity analysis was done by fitting a straight line in (f^2,t^2) space using least squares.

The results for case 1 are shown in Figure 3.2. The conventional velocity estimates are shown as the light curve and are the same in each panel. Because of the abrupt change in velocity the conventional estimate is seen to fluctuate about the midpoint where the discontinuity occurs with a wavelength equal to a cable-length (see Figure 1.2). The peak-to-peak amplitude of the fluctuation is roughly 750 ft/sec.

The LDM results for ϵ = 0.3, 0.5, and 0.7 are shown in Figure 3.2a, b, and c respectively. In each case the LDM velocity estimate has reduced the amplitude of the fluctuation but at the expense of spreading

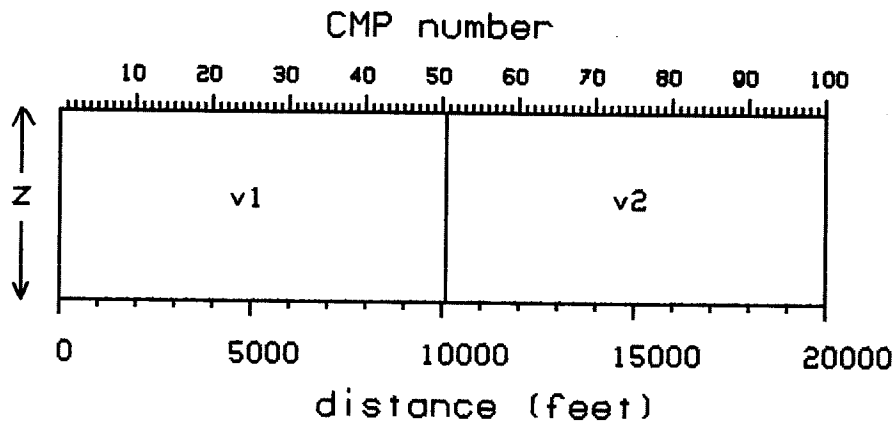

Figure 3.1. Model used to create common-midpoint traveltime data by ray tracing. The model consists of two constant velocity areas separated by a vertical boundary at x = 10100 feet (in between midpoints 50 and 51) and overlying a horizontal interface at a depth z. Traveltimes were computed for 2400% coverage across the model with a near and far offset of 400 and 9600 feet respectively. The midpoint spacing is 200 feet. Three different combinations of v_1, v_2, and z are considered (see Table 3.1).

the anomaly over a larger area. The results for the different values of ϵ appear to be very similar. On the basis of the fit at the ends of the model, however, the indication is that the larger value of ϵ does the best job.

The second case to be considered differs from the first in that the reflector depth is doubled. According to equation (2.7), this implies that the effect of the lateral velocity variations in the conventional slowness estimates should be quadrupled. Referring to Figure 3.3 (light line), this is indeed seen to be the case as the peak-to-peak amplitude of the fluctuation is now roughly 3500 ft/sec.

The LDM results are shown again as the dark lines. The difference between the different values of ϵ is now more apparent with the larger value of ϵ reducing the fluctuation amplitude the most. In each case the velocity perturbation has again been spread out over a larger area. The closer ϵ is to unity, the more the higher spatial frequencies are attenuated. Since the exact velocity function contains mostly zero

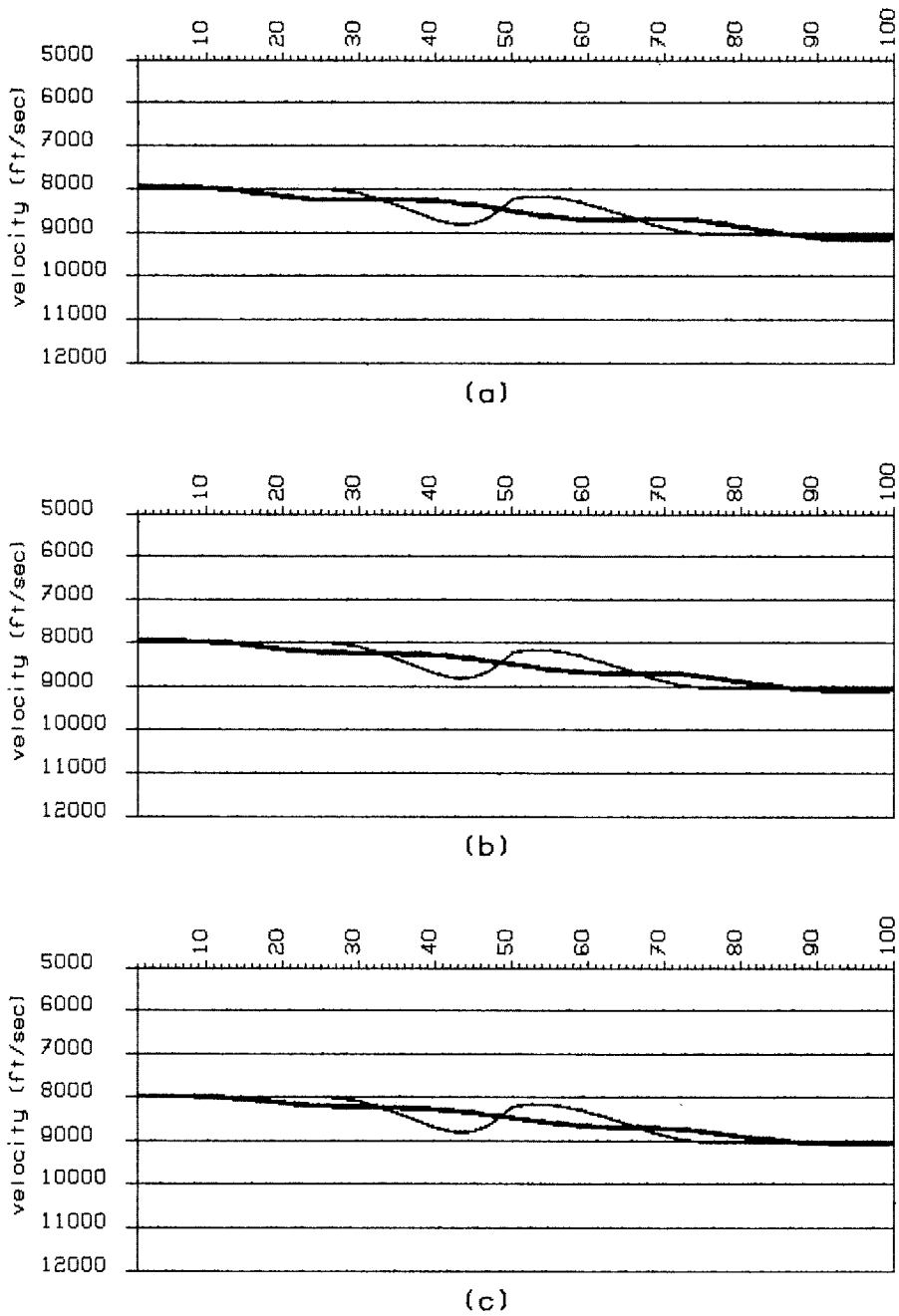

Figure 3.2. Conventional f^2,t^2 (light line) and LDM (dark line) results for Model 1 with v_1= 8000 ft/sec, v_2= 9000 ft/sec, and z = 5000 ft. The three panels are for three different values of the stability parameter ϵ : a) 0.3, b) 0.5, and c) 0.7. The correct velocity function changes abruptly between midpoints 50 and 51 from 8000 to 9000 ft/sec.

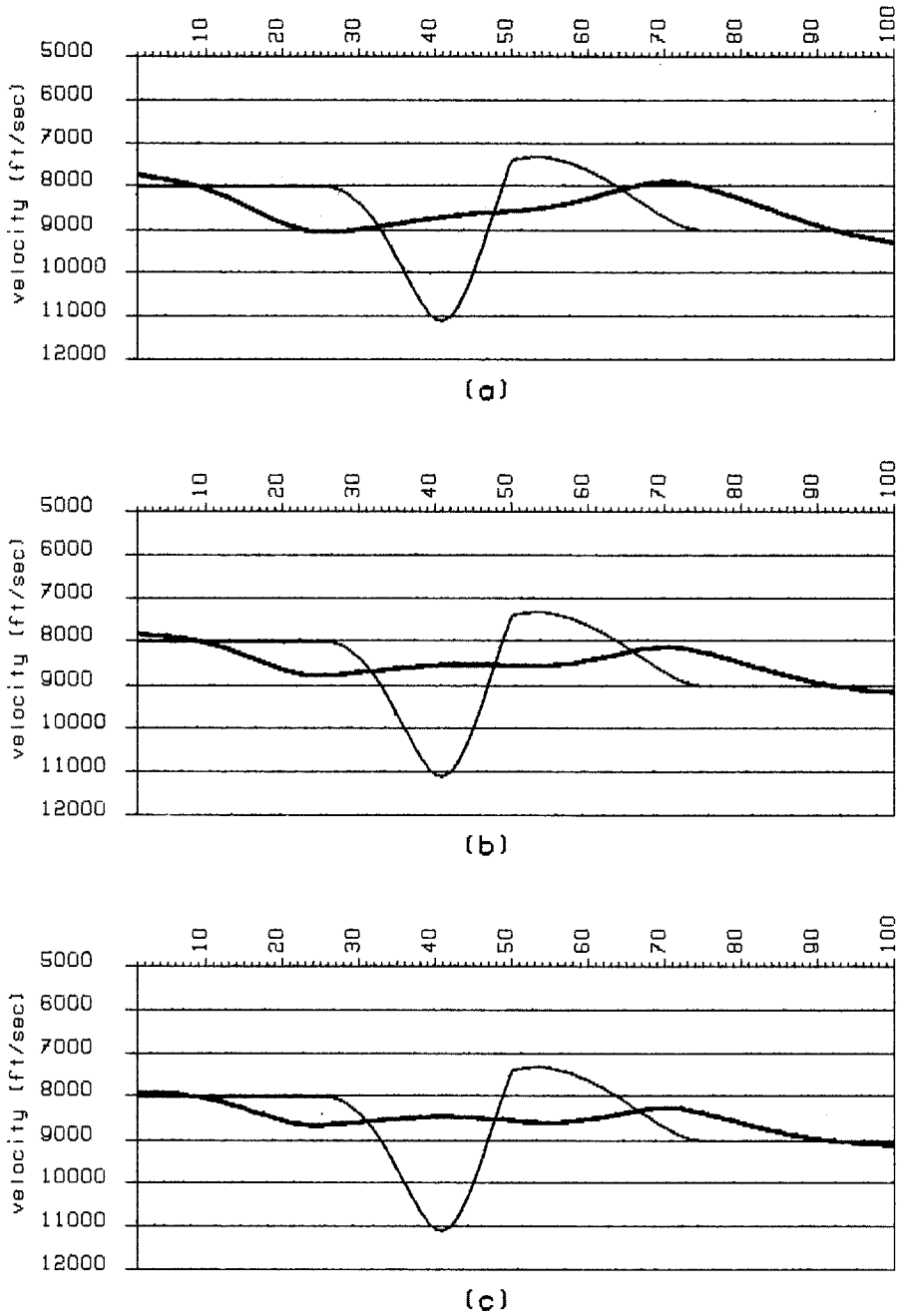

Figure 3.3. Conventional f^2,t^2 (light line) and LDM (dark line) results for Model 1 with v_1= 8000 ft/sec, v_2= 9000 ft/sec, and z = 10000 ft. The three panels are for three different values of the stability parameter ϵ : a) 0.3, b) 0.5, and c) 0.7. The correct velocity function changes abruptly between midpoints 50 and 51 from 8000 to 9000 ft/sec. The difference between this case and that shown in Figure 3.2 is in the depth z. Note that the effect of doubling the depth is to roughly quadruple the amplitude of the fluctuation of the conventional velocity estimate, as predicted by equation (2.7).

spatial frequency, it is not surprising that the larger value of ϵ gives the better result.

The final case for Model 1 differs from case 1 in that the velocity contrast is doubled across the discontinuity (v_1 = 8000, v_2 = 10000). The results from the conventional and LDM velocity estimation techniques are shown in Figure 3.4. Comparing Figures 3.2 and 3.4 indicates that doubling the velocity contrast does not adversely affect the LDM results. In fact, Figure 3.4 appears to be a scaled-up version of Figure 3.2. Once more the larger value of ϵ gives the best result, as we expected.

Based on the three cases presented we can draw the following conclusions. Over an abrupt velocity contrast the LDM substantially reduces the fluctuations in the conventional velocity estimates by spreading out the velocity anomalies. Moreover, the best results appear to come from the larger values of ϵ.

3.2. Synthetic Model 2

The purpose of the second synthetic model is to test the LDM over a region where the velocity is not homogeneous in depth. The model used for this test is shown in Figure 3.5. This is essentially the same model as that used by Pollet (1974) and consists of horizontal beds extending across the entire section with the exception of a 200-foot low velocity layer (5400 ft/sec) which begins at midpoint #100 and continues to the right of the model. Again a ray tracing method was used to generate a suite of 2400% common-midpoint gathers across the section. The midpoint and group spacing are 100 and 200 feet respectively, and the far offset distance is 5000 feet. We will estimate the vertical RMS velocity to the four interfaces below the low-velocity layer at depths 6000, 7000, 8000, and 10000 feet.

First consider the results from a conventional velocity estimation procedure shown in Figure 3.6. The correct vertical RMS velocity is shown by the light line in each panel. Again the lateral velocity discontinuity manifests itself as large fluctuations in the velocity

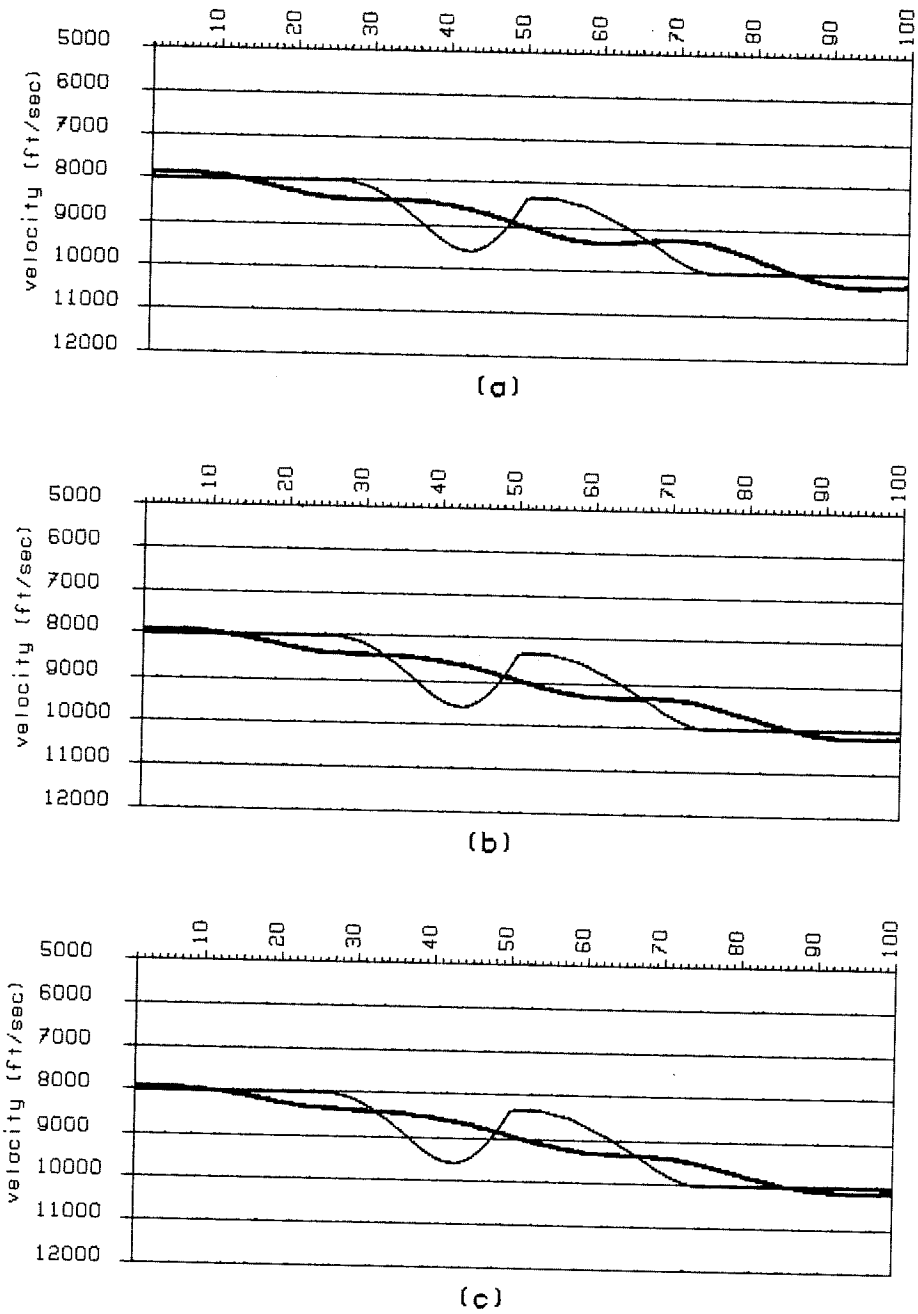

Figure 3.4. Conventional f^2,t^2 (light line) and LDM (dark line) results for Model 1 with v_1 = 8000 ft/sec, v_2 = 10000 ft/sec, and z = 5000 ft. The three panels are for three different values of the stability parameter ϵ : a) 0.3, b) 0.5, and c) 0.7. The correct velocity function changes abruptly between midpoints 50 and 51 from 8000 to 10000 ft/sec.

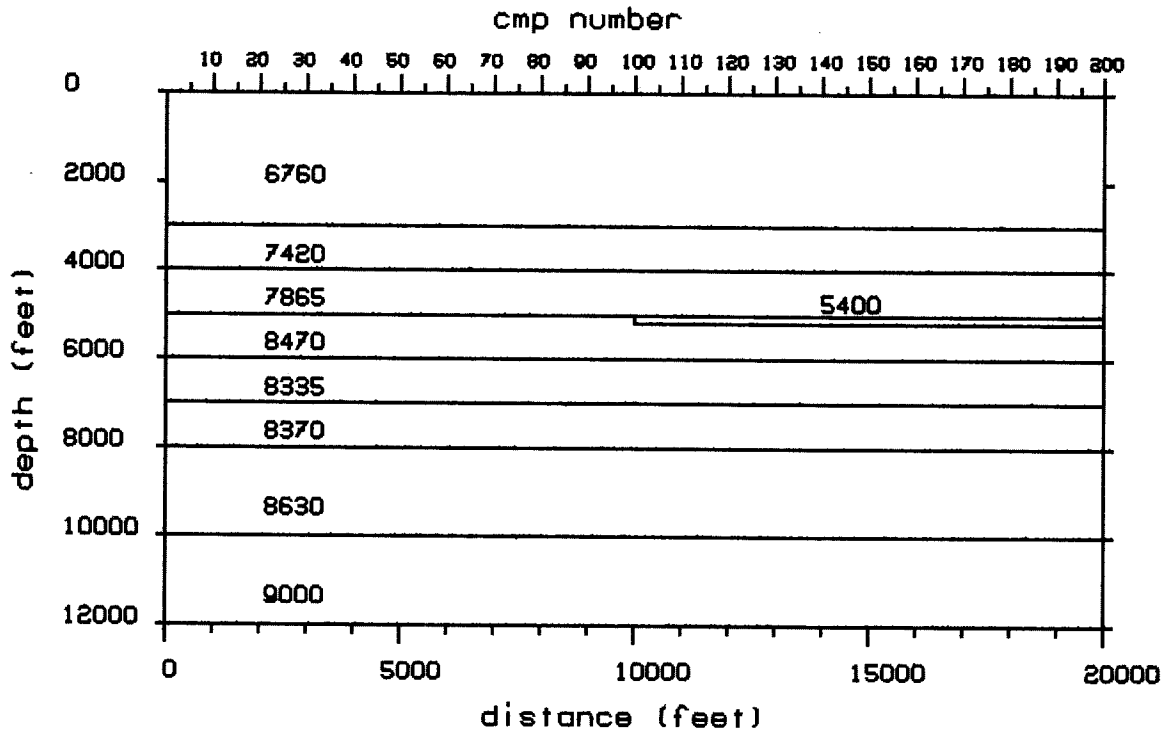

Figure 3.5. Model 2. Model used to test the LDM over a region of vertical velocity inhomogeneity (adapted from Pollet, 1974). The velocities of the layers are given in ft/sec. Traveltimes for the common-midpoint gathers were generated using a ray tracing program with locations shown at the top of the figure. The CMP gathers are 24-fold with a midpoint spacing of 100 feet and a group spacing of 200 feet. Distance to the far offset is 5000 feet. The discontinuity occurs at CMP #100.

estimates. Two features of the conventional velocity estimation results are of special interest. First the amplitude of the velocity fluctuation increases with depth as expected from equation (2.7) and from the previous model. Second, the width of the fluctuaton increases with depth as a result of the velocity discontinuity not extending from the surface to each reflector.

Because of the fluctuations in RMS velocity, the implied interval velocities will also be in error. For example, Figure 3.7 shows the estimated interval velocities for the layer between 6000 and 7000 feet using the RMS velocities in Figures 3.6a and 3.6b and Dix's equation

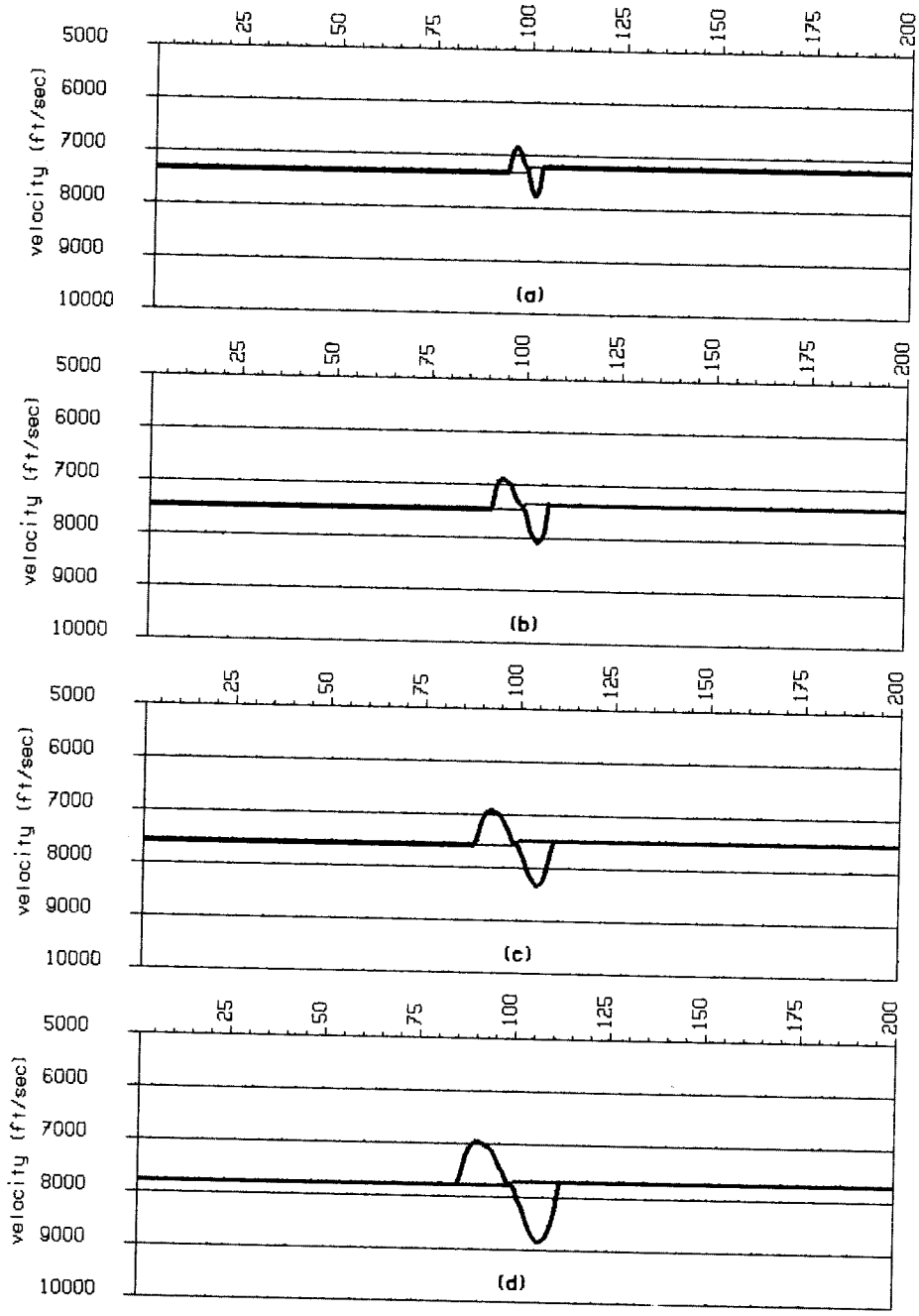

Figure 3.6. Conventionally estimated (bold lines) and true (light lines) RMS velocities to the interfaces at 6000, 7000, 8000, and 10000 feet in Model 1. Numbers at the top refer to the CMP numbers in Figure 3.5. The low velocity zone discontinuity occurs at CMP #100 and its effect is seen as causing the large fluctuations in the velocity estimates. Ideally, the RMS velocity should change abruptly at CMP #100, being slightly lower on the right.

$$v_{int}^2 = \frac{\bar{v}_b^2 t_b - \bar{v}_a^2 t_a}{t_b - t_a} \tag{3.1}$$

where $\bar{v}_a$ and $\bar{v}_b$ are the RMS velocities from Figures 3.6a and 3.6b respectively and t_a and t_b are the associated two-way traveltimes. The correct velocity should remain constant at 8335 ft/sec across the section, as seen in Figure 3.5. We see, however, that the estimated interval velocities are very unreliable in the vicinity of the truncation ranging from as low as 2000 ft/sec to as high as 12,400 ft/sec.

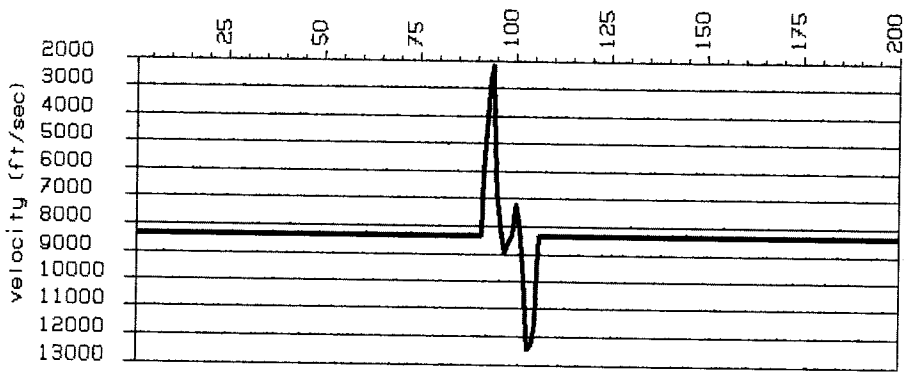

Figure 3.7. Estimated interval velocity in the 6000 to 7000-foot layer in Model 2 using the estimated RMS velocities in Figures 3.6a and 3.6b and Dix's equation. The correct interval velocity is 8335 all the way across the section.

One possible means of reducing the RMS velocity fluctuations, as discussed by Pollet (1974) and Schneider (1971), is to smooth the velocity functions by performing a lateral average on the velocities. The results from one such smoothing operator are shown in Figure 3.8. The light lines are the correct vertical RMS velocities and the heavy lines are the smoothed results. In this example, the averaging was done on two passes with eight adjacent velocity functions averaged together followed by an averaging of five adjacent smoothed velocity functions. The smoothing did a reasonable job of removing the short wavelength velocity variations for the reflector at 6000 feet, but only marginally improved the estimates for the deeper reflectors. In fact, in order to smooth

the curve for the 10000-foot reflector, it is necessary to average perhaps 80 to 100 adjacent midpoints. Clearly, smoothing is a subjective operation with no criteria on how much smoothing should be done. Moreover, smoothing the velocities will reduce any lateral resolution that existed to begin with.

The interval velocities for the layer between 6000 and 7000 feet show some improvement when the smoothed velocities are used (Figure 3.9). There still exists, however, a considerable amount of error in the vicinity of the discontinuity at midpoint #100.

In applying the LDM to Model 2, the conventional velocity estimates were first extended on both sides with the value of the endpoints to yield an input dataset of 512 midpoints to assure no boundary condition contamination in the solution. The results are shown in Figure 3.10. The value of the stability parameter, ϵ, is 0.5.

For the interfaces at 6000 and 7000 feet (Figure 3.10a,b), the LDM velocity estimates show only a negligible error. This is mainly due to the high spatial frequencies of the anomaly which get nearly completely attenuated in the inversion. The high quality of the velocity estimates is reflected in the implied interval velocity shown in Figure 3.11 where only a slight fluctuation remains in the estimate.

For the two deeper interfaces (Figure 3.10c,d), where the wavelength of the velocity fluctuation is larger, the LDM leaves a noticeable error in the estimate but still is substantially better than the conventional and smoothed conventional velocity estimates. Again, we cannot expect the LDM to recover the high spatial frequencies of the true solution.

The results shown in Figure 3.10 indicate that the vertical homogeneity assumption in the development of the lateral derivative travel-time equations does not adversely affect the LDM results.

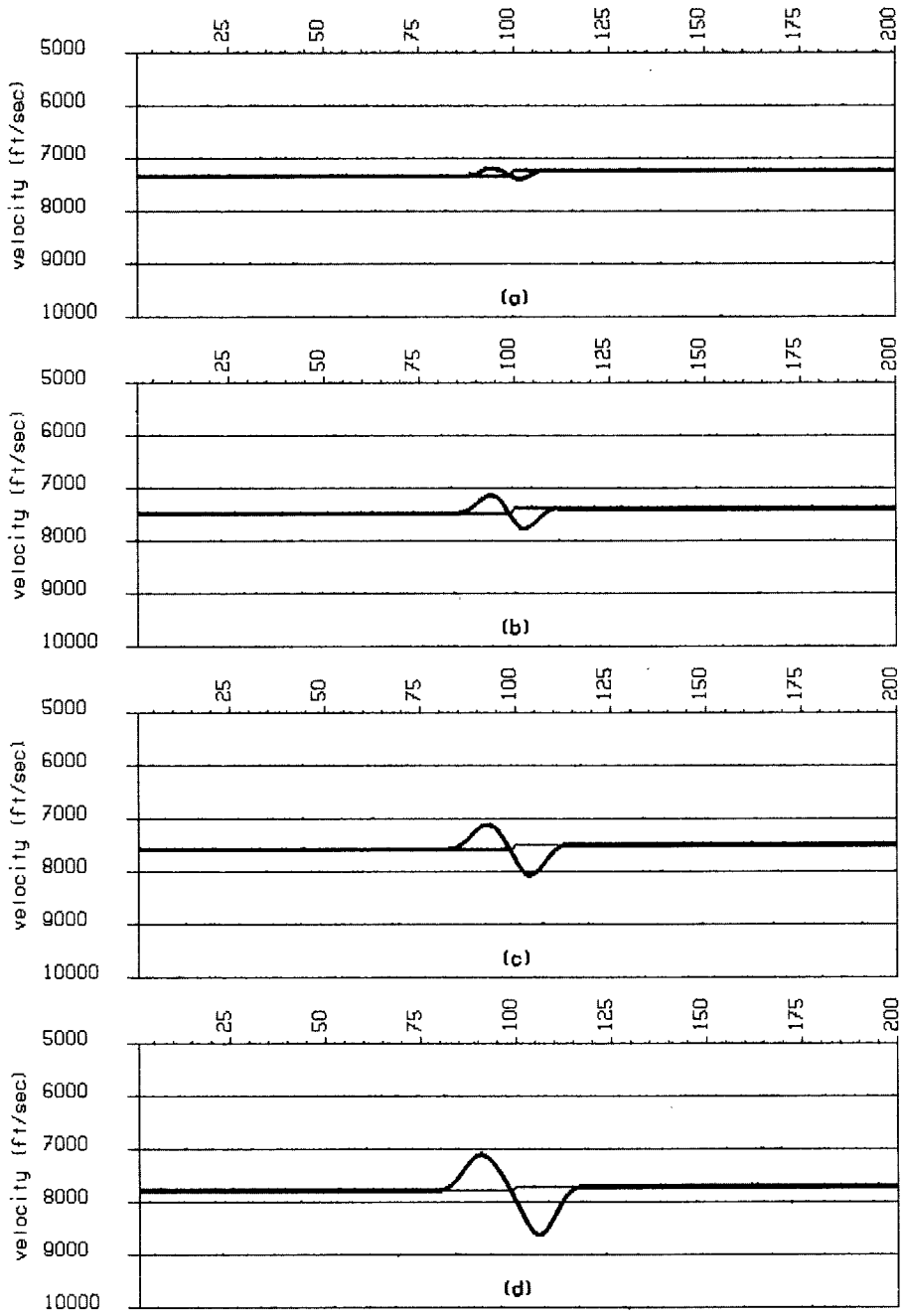

Figure 3.8. Smoothed version of the velocity estimates in Figure 3.6. The light line in each figure is the correct velocity. The bold line is a smoothed version. In this example, smoothing was done by averaging eight adjacent midpoints followed by an averaging of 5 adjacent smoothed velocities. Only the velocity estimates for the interface at 6000 feet appear to be reasonable after the smoothing. The deeper horizons would require much more smoothing to remove the large fluctuations. The problem is, however, how does one know when enough, or too much, smoothing has been done?

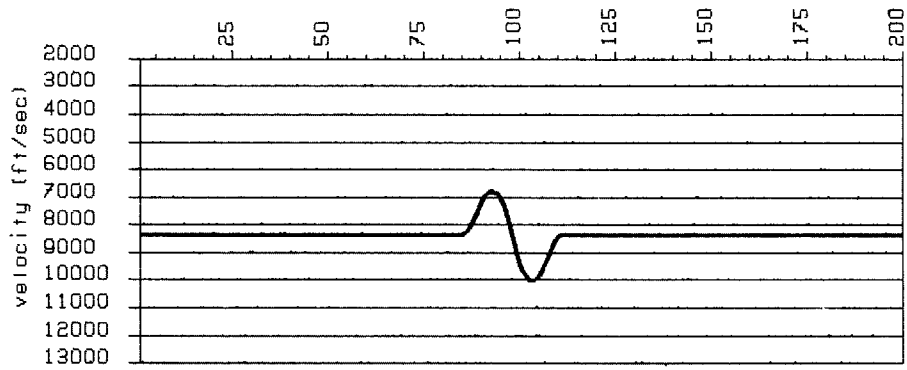

Figure 3.9. Estimated interval velocity for the 6000 to 7000-foot layer in Model 2 using the smoothed conventionally estimated RMS velocities in Figures 3.8a and 3.8b. The correct interval velocity is 8335. Compare with Figure 3.7.

3.3. Synthetic Model 3

Both of the synthetic models considered up to this point have been relatively simple in that they consist of flat reflectors and contain no velocity gradients across the section. The purpose of this section is to test the LDM in an area where there are regional gradients in velocity to see if the LDM will pick them out. The model for this test is shown in Figure 3.12 and consists of four regions of constant velocity separated by irregular interfaces. We will concern ourselves with estimating the vertical RMS velocity to the horizon at 8000 feet. As with the previous models, the traveltimes for 24-fold common-midpoint geometry were generated across the model with a ray tracing procedure. The near and far offsets are 400 and 9600 feet respectively with a midpoint spacing of 200 feet.

A standard f^2,t^2 velocity estimation was first done on the traveltimes to this horizon and the results are shown in Figure 3.13. The true vertical RMS velocity to this interface is shown as the lighter line. Although the interface is horizontal in depth, it is not in time, which accounts for most of the discrepancy between the true and estimated RMS velocities between midpoints 70 to 115 and 145 to 240. Around midpoints 50, 130, and 270 the conventional velocity measure

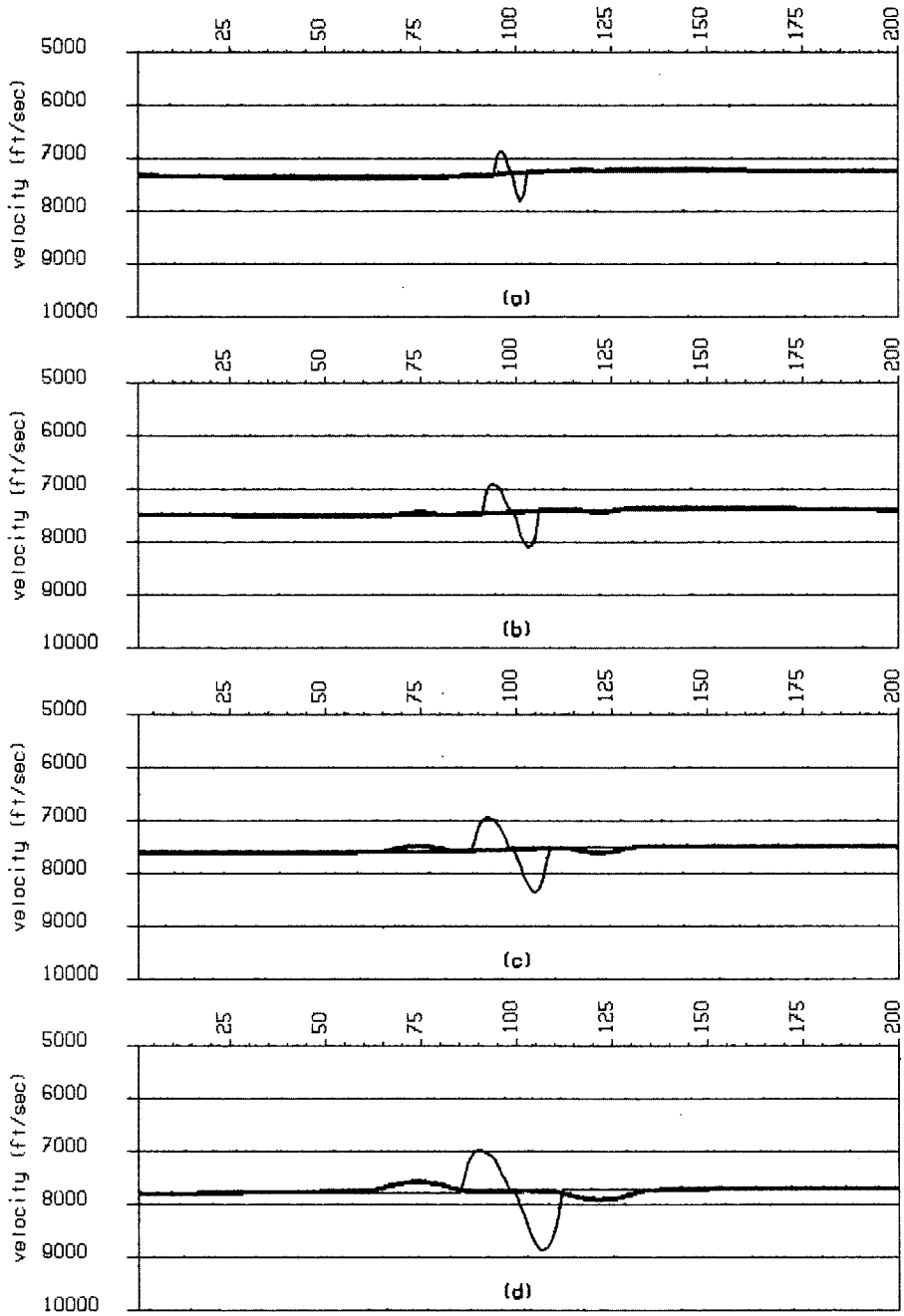

Figure 3.10. LDM results for Model 2. Estimated RMS velocities (bold lines) to the interfaces at 6000, 7000, 8000, and 10000 feet in Figure 3.5 using the traveltimes to the offsets at 400 and 2800 feet. The light line is the unsmoothed conventional velocity estimates from Figure 3.6.

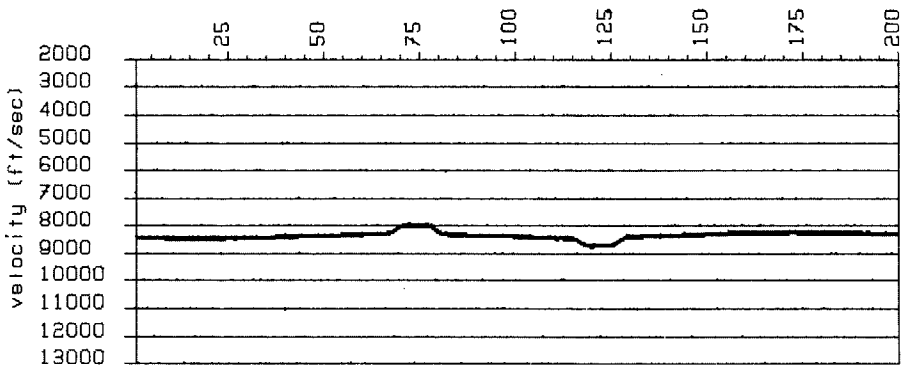

Figure 3.11. Estimated interval velocity for the 6000 to 7000-foot layer in Model 2 using the estimated RMS velocities in Figure 3.10a and 3.10b and Dix's equation. The correct interval velocity is 8335 ft/sec. Compare with Figures 3.7 and 3.9.

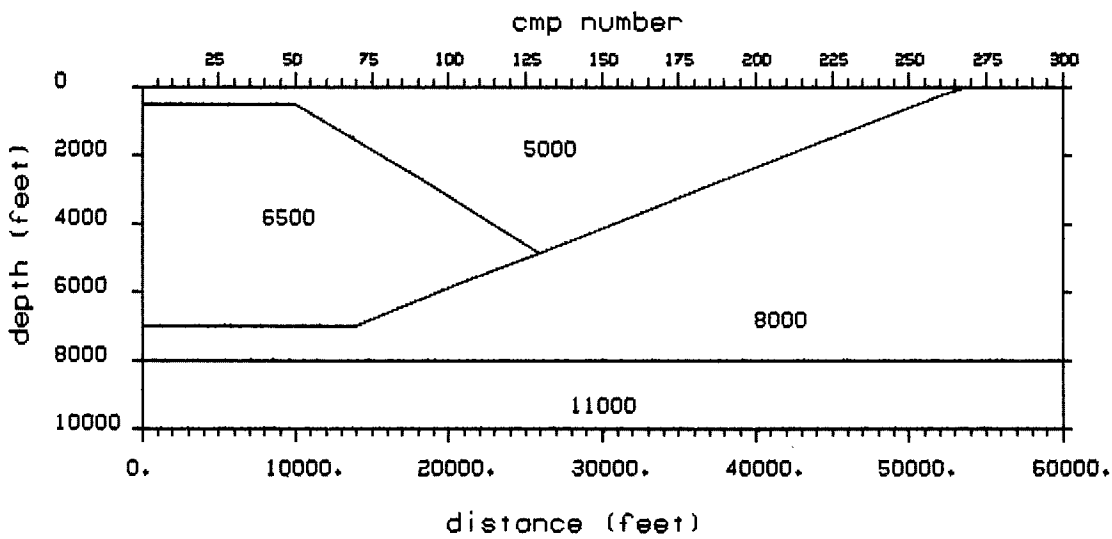

Figure 3.12. Model 3. Traveltimes were generated for a 24-fold common-midpoint geometry for the midpoints shown at the top. The near and far offsets are 400 and 9600 feet respectively with a midpoint spacing of 200 feet. Velocities are given in ft/sec.

gives a poor estimate of the true velocity because of the large lateral second derivative in velocity. It can be seen from Figure 3.13, as well as verified from Equation (2.7), that the conventional ***velocity*** estimate is too low when w" > 0 and too high when w" is < 0.

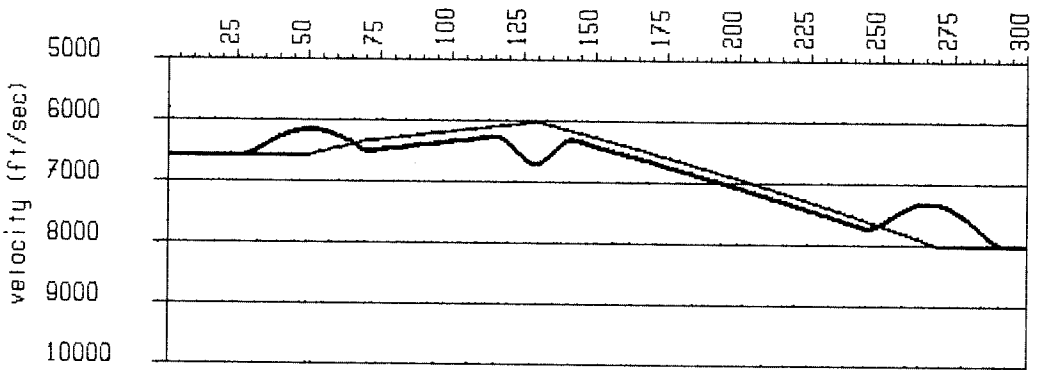

Figure 3.13. Conventional velocity estimation results (bold line) for the interface at z = 8000 feet in Model 3. The true vertical RMS velocity is shown by the lighter line.

As with the previous two models, the conventional velocity estimates were first extended on both sides of Model 3 with the value of the endpoints to yield an input dataset of 512 midpoints to the LDM. The results from the LDM are shown in Figure 3.14 for three values of the stability parameter, ϵ.

For ϵ = 0.5 (Figure 3.14a), the LDM result does not show much improvement over the conventional velocity estimate, especially on the right-hand side of the model. Morevover, the velocity function appears to oscillate around the midpoints with the large second lateral derivatives of velocity. The result does seem to pick up the regional trend in velocity, however.

Increasing ϵ to 0.7 and 0.9 (Figure 3.14b,c) improves the LDM result substantially, with the latter showing the best result. In between midpoints 150 and 235, where there is a monotonic decrease in velocity, the LDM results match the gradient very well. Thus, the LDM

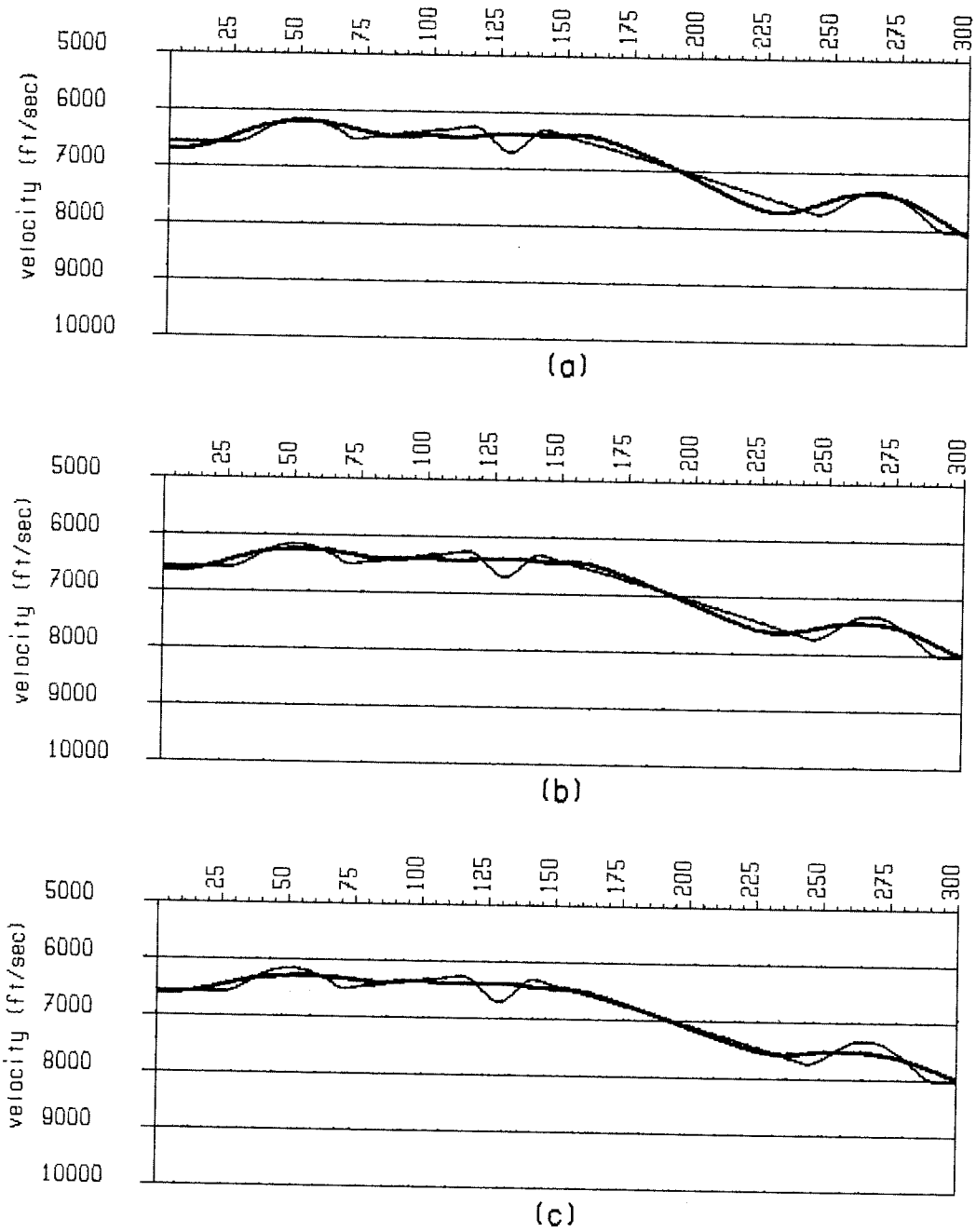

Figure 3.14. LDM results for Model 3. The three cases shown are for a) ϵ = 0.5, b) ϵ = 0.7, and c) ϵ = 0.9.

does appear to pick out the regional gradients in velocity even though they are neglected in the derivation of the traveltime equations. Note that the LDM, like conventional methods, will yield a velocity estimate which is not dip corrected (see Levin, 1971) and must be compensated for with a cos(dip) correction in order to yield the true RMS velocity.

3.4. Field data test

As a final example, we will apply the LDM to a marine field dataset. The data used are from the Grand Banks area off the coast of Newfoundland. A stacked section is shown in Figure 3.15. The CMP gathers are 24-fold and collected at a sample rate of 4 msec. The midpoint spacing is 164 feet and the cable-length is 8570 feet or roughly 52 midpoints. The horizon of interest is a strong reflector between 2 and 3 seconds dipping from right to left with a dip of approximately 2 degrees. On the larger section from which this data is taken, the horizon appears to be straight so that the undulations are assumed to be caused by the seafloor topography. The trough in the seafloor in Figure 3.15 spans roughly two to three cable-lengths. The bump at the bottom of the trough is an out-of-plane reflection.

A conventional velocity analysis was done at every midpoint along the section by picking the peaks of a semblance contour map, and these results are shown as the bold line in Figure 3.16a. The high spatial frequency jitter in the velocity function is due to the resolution in picking the RMS velocities and cannot be considered real. The effect of the seafloor topography is to create fluctuations in the velocity function with wavelengths on the order of a cable-length. These fluctuations are also too high in spatial frequency to place any confidence in them and can be considered artifacts of the lateral velocity variation. The light curve in Figure 3.16a is a smoothed version of the conventional velocity estimates where the velocities were averaged over one cable length.

Using a water velocity of 5000 ft/sec, the zero-offset times to the seafloor and the reflector, and equation (3.1), the interval velocity functions shown in Figure 3.16b are obtained for the unsmoothed (bold

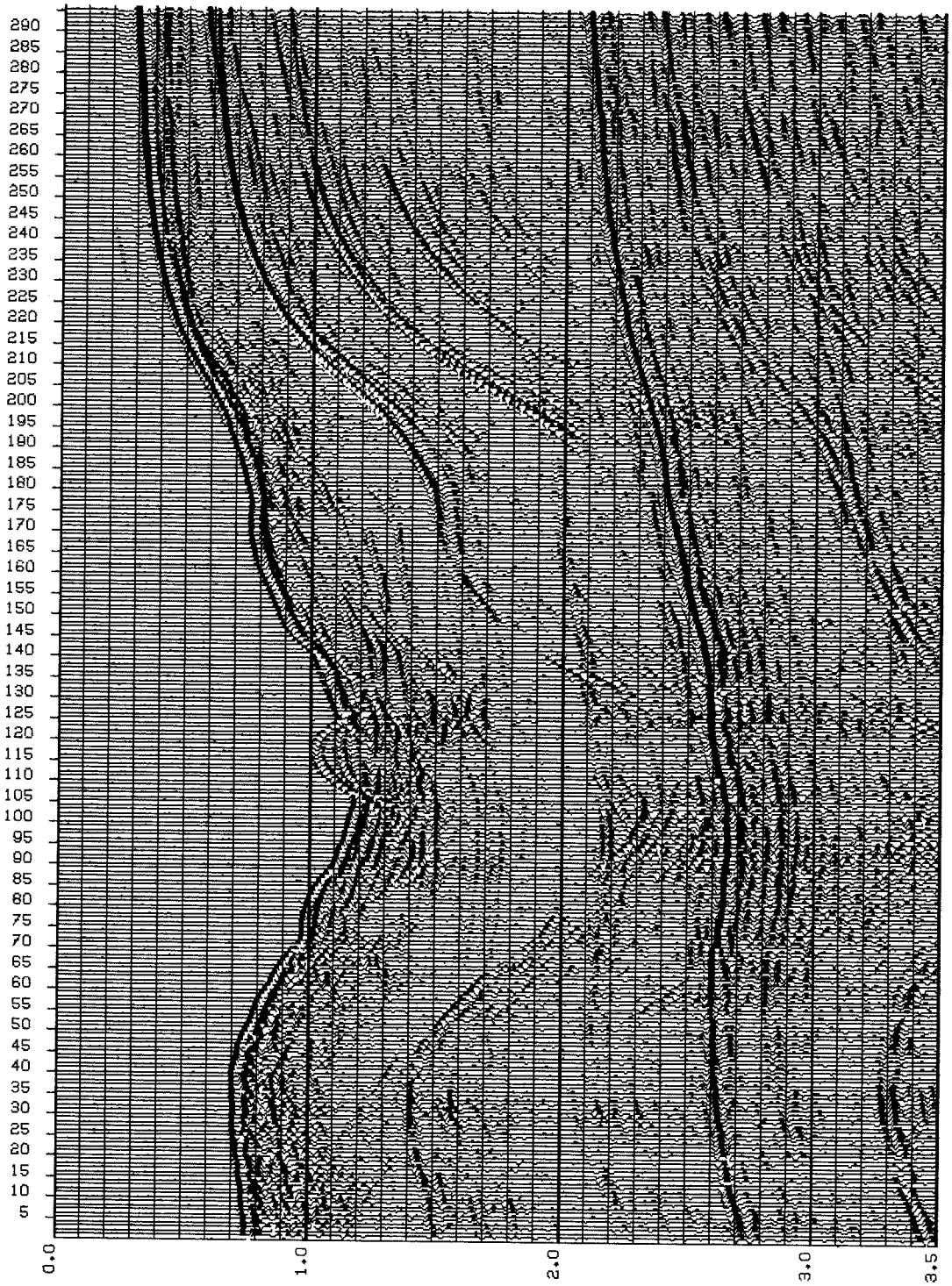

Figure 3.15. Stacked section of marine data collected over the Grand Banks area. The midpoint numbers at the top correlate with those in Figures 3.16 - 3.21. The midpoint spacing is 164 feet and the cable-length is 8570 feet or roughly 52 midpoints. The horizon of interest is the strong event between 2.1 and 2.8 seconds and dipping from right to left.

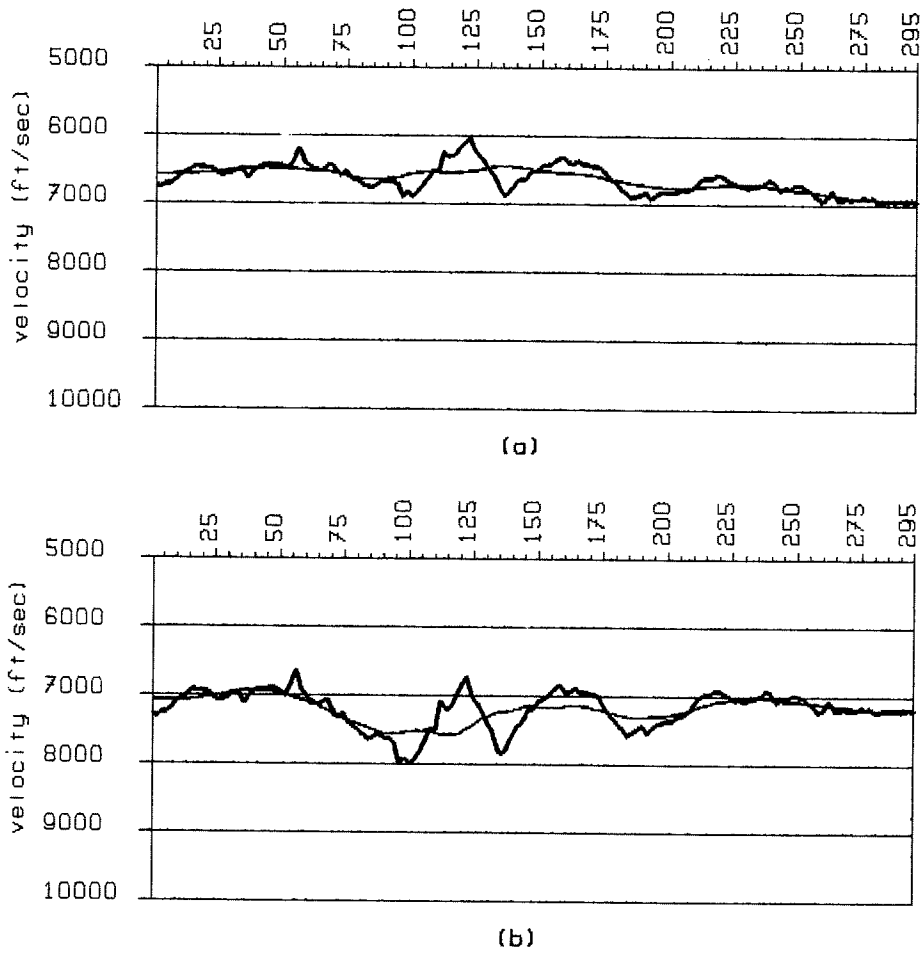

Figure 3.16. Field data conventional and smoothed velocity estimates. a) RMS velocity to the strong reflector between 2 and 3 seconds in Figure 3.15. b) Interval velocity between the seafloor and the strong reflector using equation (3.1).

line) and the smoothed (light line) velocity functions.

The application of LDM is identical to the application in the synthetic models of the previous sections. The input data are the RMS velocities in Figure 3.16a. Before inverting equation (2.32) these data were first extended on both sides of the section to give a total input data vector of 512 midpoints. Also, the RMS velocity estimates were first smoothed over a cable-length, so the actual function from which the second lateral derivatives were computed is the light line in Figure 3.16a.

Two results from the LDM are shown. The first is for a stability parameter of ϵ = 0.7 and is shown in Figure 3.17 superimposed on the unsmoothed conventional velocity curve. The LDM result is similar to the smoothed curve in Figure 3.16, but contains some of the shorter wavelength fluctuations. The similarity results because the amount of lateral fluctuation in the smoothed stacking velocity function in Figure 3.16 is not very great (<400 ft/sec) and consequently the LDM is not expected to do very much to it. The corresponding interval velocity is shown in Figure 3.17b.

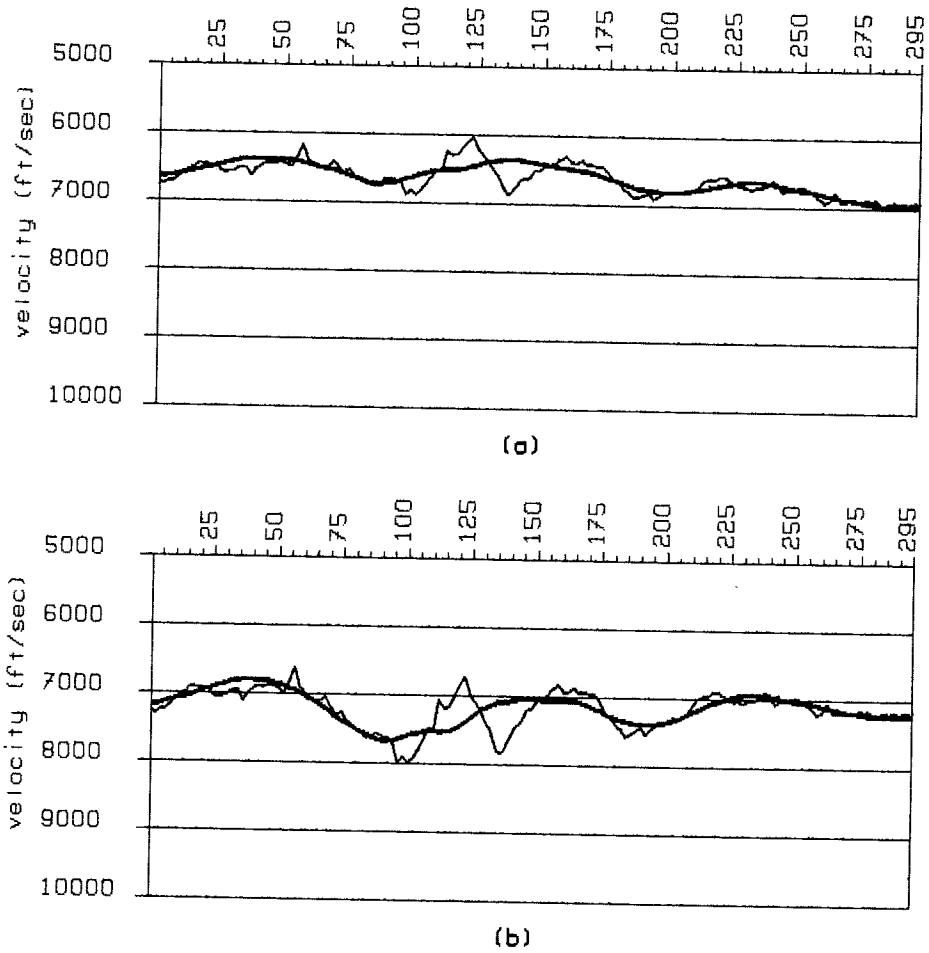

Figure 3.17. LDM results with ϵ = 0.7: a) RMS velocity b) interval velocity.

Figure 3.18 shows the LDM result for ϵ = 0.9. The result is nearly identical with the smoothed version of the conventional velocity result in Figure 3.16. It is interesting to note that the minimum in the RMS velocity function (approximately midpoint #135) does not occur over the center of the trough in the seafloor which is at midpoint #105. This raises the question of the validity of the LDM results.

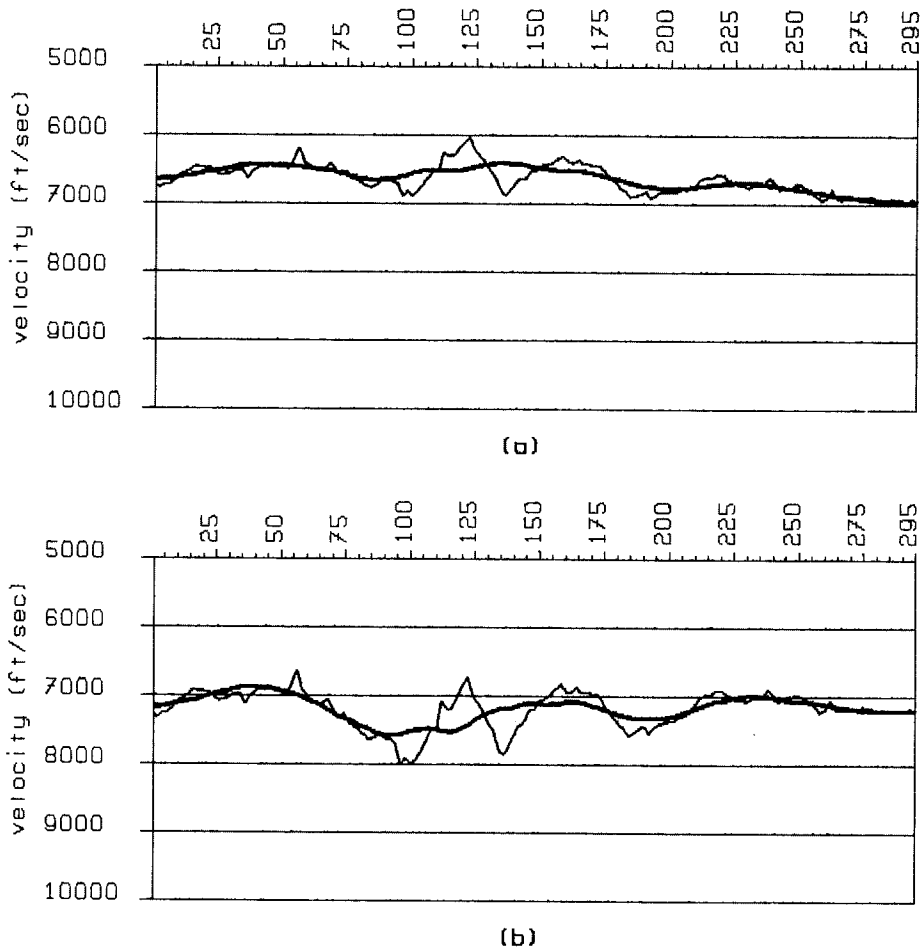

Figure 3.18. LDM results with ϵ = 0.9: a) RMS velocity b) interval velocity.

The LDM velocity estimates can be tested by performing a depth migration on the stacked data in Figure 3.15. The depth migration is done with a variable velocity 45-degree finite-difference algorithm where the lateral velocity variations are accounted for with a space- and time-varying shifting term (see Claerbout, 1976). The input model used in the depth migration is shown in Figure 3.19. Only two velocities are used: 5000 ft/sec for the water and 7200 ft/sec for the sediments. If the sediment velocity is indeed constant then after migration the reflector will appear straight. If the reflector is not straight after the migration, then the true sediment velocity must vary laterally as the effect of the seafloor topography will be removed.

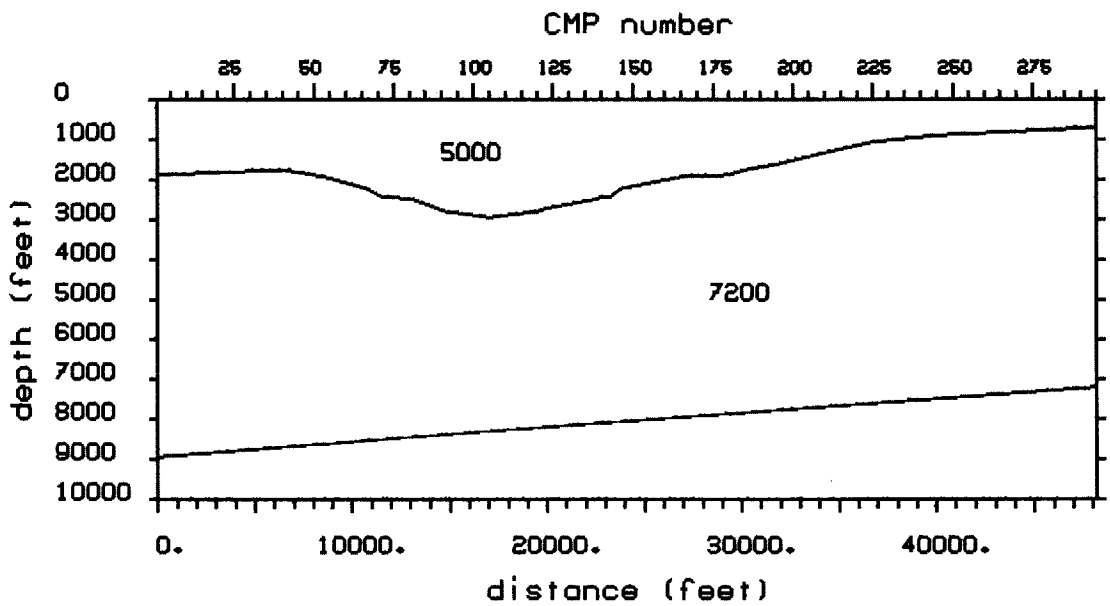

Figure 3.19. Velocity model for depth migration.

The migrated depth section is shown in Figure 3.20. The vertical axis is in kft. Sighting along the reflector it is seen that it is not straight after the migration but deviates on the order of 100 to 200 feet from a straight line. This is more easily seen in Figure 3.21, which shows an expanded view of the 7 to 10 kft portion of the section. Comparing the LDM results in Figures 3.17 and 3.18 with the migrated sections shows that there is indeed a correlation between the fluctuations in the interval velocity and the departure of the migrated reflector from a straight dipping bed. For example, around midpoint #150 there is a relative minimum in the interval velocity curve. On the migrated section the reflector appears to be low in this vicinity implying it was migrated at a slightly too high velocity. Also around midpoints #100 to #110 there is a relative maximum in the interval velocity function which corresponds to a slight relative undermigration of the bed in Figure 3.21.

Interval velocity calculations are very sensitive to noise and in the case shown are no more accurate than 100 to 200 ft/sec. However, the correlation between the LDM interval velocity and the fluctuations in the dipping reflector do seem real.

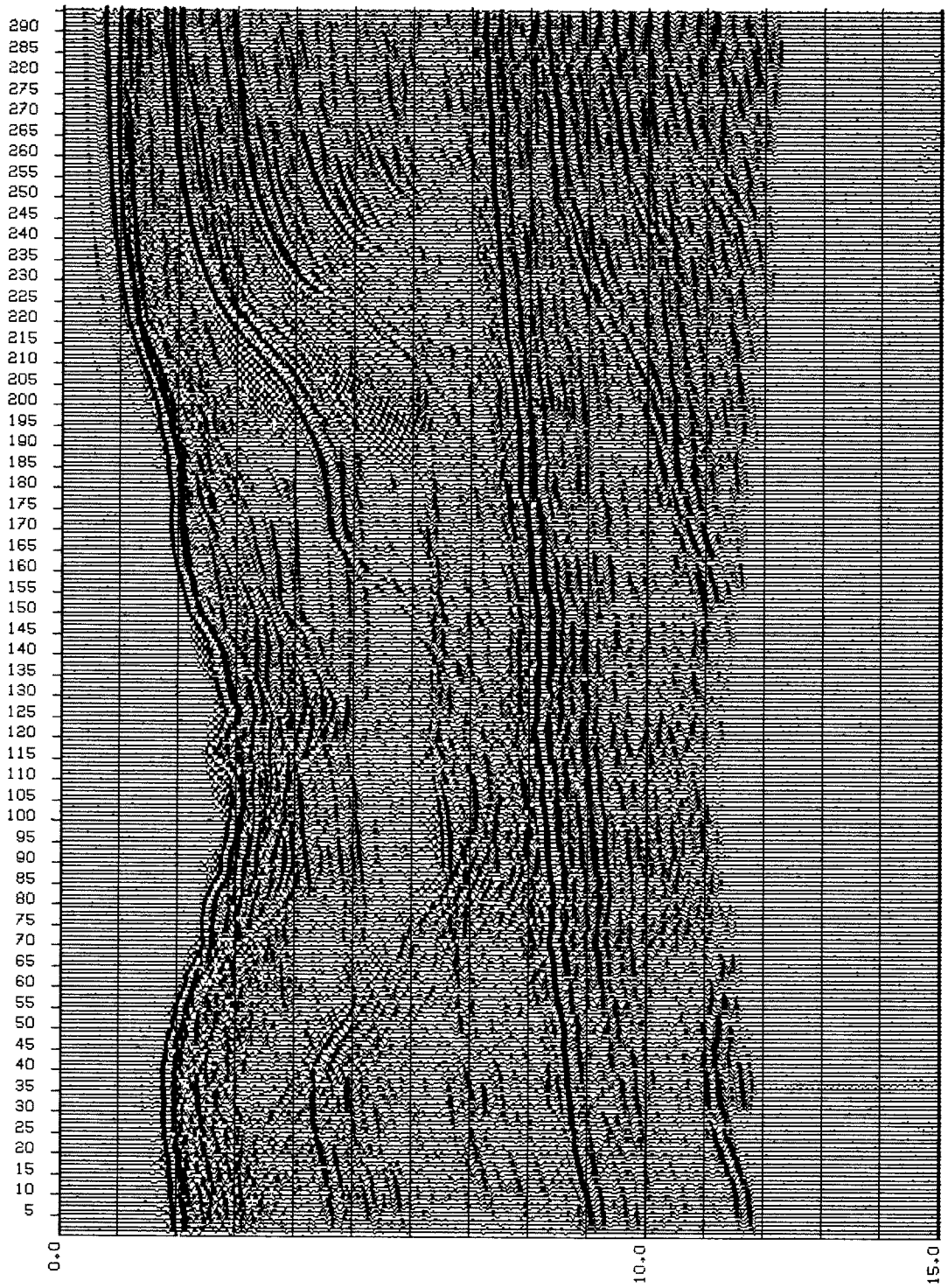

Figure 3.20. Depth migration of the stacked section in Figure 3.15. The vertical axis is in kft.

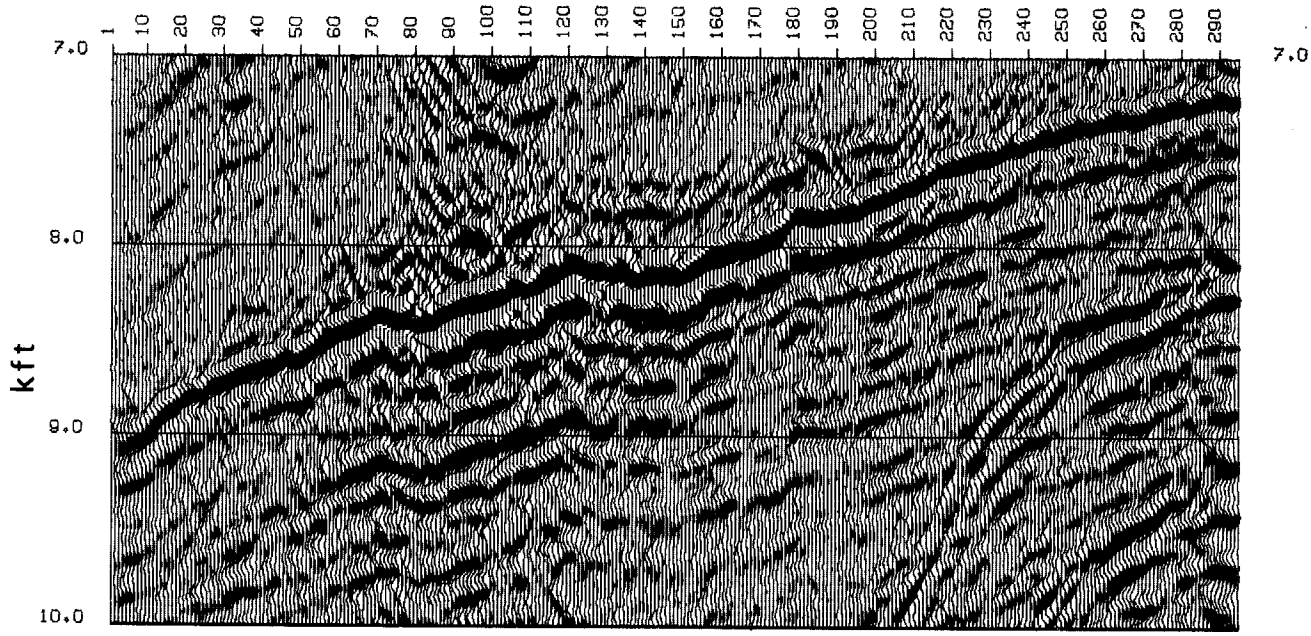

Figure 3.21. Expanded view of the 7 to 10 kft level of the depth migration in Figure 3.20.